Chem

CellPress

Article

Highly Fluorinated Interphases Enable High-Voltage Li-Metal Batteries

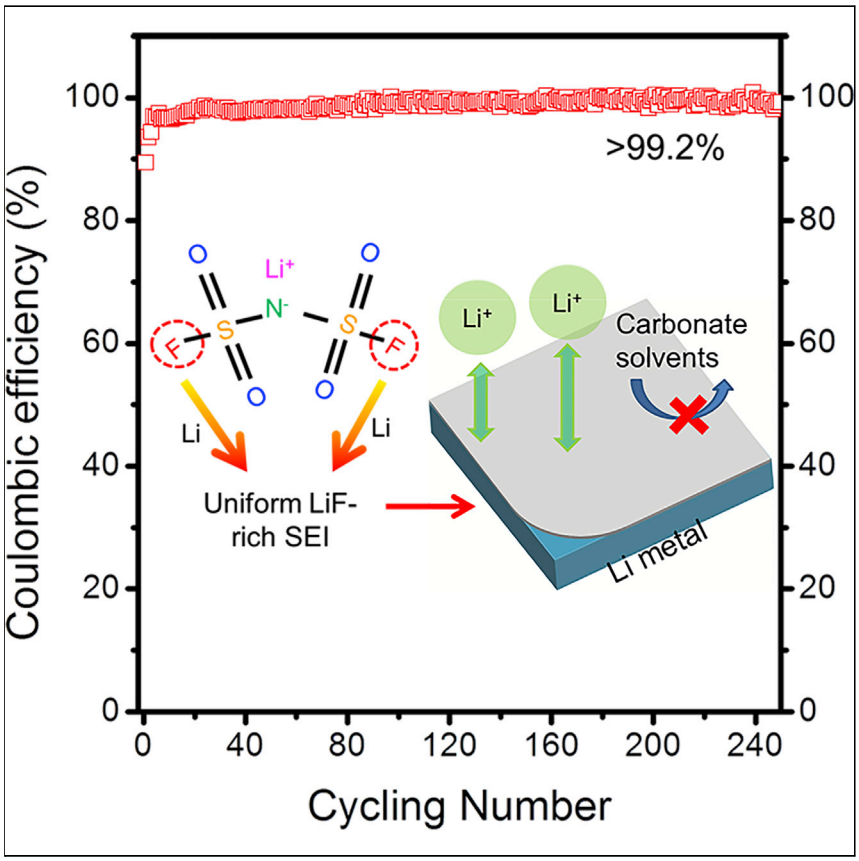

Li metal is regarded as the "Holy Grail" electrode because of its highest specific capacity and lowest electrochemical potential. However, challenges arising from the low Coulombic efficiency (CE) and dendritic nature of Li metal in carbonate electrolytes remain to be resolved. Here, by increasing LiFSI salt concentration in the carbonate electrolyte, we successfully increased the CE to ~99.3% while suppressing Li dendrite formation. An NMC622||Li cell was paired and showed excellent cycling performance.

Xiulin Fan, Long Chen, Xiao Ji, ..., Jianjun Jiang, Kang Xu, Chunsheng Wang

cswang@umd.edu

HIGHLIGHTS

High Li plating/stripping Coulombic efficiency was achieved in carbonate electrolytes

In-situ-formed LiF-rich SEI successfully suppresses Li dendrite growth

Ni-rich cathode is paired with Li-metal anode in the electrolytes and cycles well

Fan et al., Chem 4, 174–185
January 11, 2018 © 2017 Elsevier Inc.
https://doi.org/10.1016/j.chempr.2017.10.017

Chem

CellPress

Article

Highly Fluorinated Interphases Enable High-Voltage Li-Metal Batteries

Xiulin Fan,[1] Long Chen,[1] Xiao Ji,[1] Tao Deng,[1] Singyuk Hou,[1] Ji Chen,[1] Jing Zheng,[1] Fei Wang,[1] Jianjun Jiang,[2] Kang Xu,[3] and Chunsheng Wang[1,4,*]

SUMMARY

We were able to demonstrate excellent cycling performance of Li-metal anodes in carbonate electrolytes by increasing the Li bis(fluorosulfonyl)imide (LiFSI) concentration to ~10 M. The high concentration (10 M) of FSI anion enabled interphases of high F content on both Li-metal anode and Ni-rich NMC (nickel-manganese-cobalt) cathode surfaces. Such F-rich interphases effectively suppressed Li dendrite formation, as demonstrated by a high Li plating/stripping Coulombic efficiency of ~99.3%, and stabilized the carbonate molecules against oxidation at high cutoff voltages of 4.6 V on the surface of $LiNi_{0.6}Mn_{0.2}Co_{0.2}O_2$ (NMC622). The combination of unique stabilization on both Li-metal anode and NMC622 cathodes enabled high-energy Li-metal batteries constructed on the aggressive chemistry. Under the harsh conditions of a high charge voltage of 4.6 V and high loading of 2.5 mAh/cm^2, the NMC622||Li cells retained ~86% of their original capacity after 100 cycles. The electrolyte strategy presented here offers unique guidelines for further optimizing beyond Li-ion chemistries.

INTRODUCTION

Although they dominate the consumer electronics market and are penetrating the electric vehicle market, Li-ion batteries (LIBs) are approaching the upper limit of energy densities that intercalation chemistries can provide.[1] State-of-the-art LIBs with the typical graphite and $LiCoO_2$ as anode and cathode can deliver a specific energy of ~250 Wh/kg, which is an order of magnitude lower than gasoline can deliver.[2] To further enhance the energy density of batteries, more aggressive chemistries are required, one of which is a Li-metal anode. When coupled with a high Ni-content cathode such as $LiNi_{0.6}Mn_{0.2}Co_{0.2}O_2$ (NMC622), a 500 Wh/kg battery becomes possible.

Li metal is considered the ultimate anode material because of its unique combination of the highest specific capacity of 3,860 mAh/g and the lowest electrochemical potential (−3.04 V versus standard hydrogen electrode) ever possible from any known materials.[2–6] However, its notoriety in both chemical and electrochemical stability, as demonstrated by limited Coulombic efficiency (CE) and dendrite formation during cycling, prevents its application in a battery environment.[7–14] Extensive work has been devoted to stabilizing Li-metal anodes through approaches including protective layers,[15–18] electrode designs at nanoscale,[19–22] electrolyte additives,[14,23–27] and solid-state electrolytes[15,28]. Among these, ether-based electrolytes present the highest CE and the lowest overpotential, effectively suppressing dendrite growth owing to their low reactivity with Li metal.[2,4,12,14,17,22,29–35] Especially, the highest cycling CE of 99.1% was recently realized in 1,2-dimethoxyethane (DME).[4] However, ether-based electrolytes are intrinsically unstable against oxidation on cathode surfaces, as characterized by their typical anodic limits of <4 V,[36] which is much lower

The Bigger Picture

Interest in Li-metal batteries (LMBs) is reviving because higher energy densities can be enabled by the highest specific capacity and the lowest electrochemical potential of a Li-metal anode. However, challenges arising from the low Coulombic efficiency (CE) and dendritic nature of Li metal in carbonate electrolytes remain to be resolved. Here, by increasing LiFSI concentration in carbonate electrolytes (dimethyl carbonate [DMC], propylene carbonate, and ethylene carbonate/DMC) to 10 M, we achieved a high CE (~99.3%) of Li deposition and stripping, along with an anodic stability of >5.5 V. Pairing a Li-metal anode in this electrolyte with $LiNi_{0.6}Mn_{0.2}Co_{0.2}O_2$ (NMC622) at high loading (2.5 mAh/cm^2) created a NMC622||Li cell, which showed a high capacity retention of 86% after 100 cycles at a high cutoff voltage of 4.6 V. LiF-rich and F-rich interphases formed on the Li-metal anode and cathode surfaces, respectively, are responsible for the successful suppression of Li dendrite growth as well as stabilization of the high-voltage cathode.

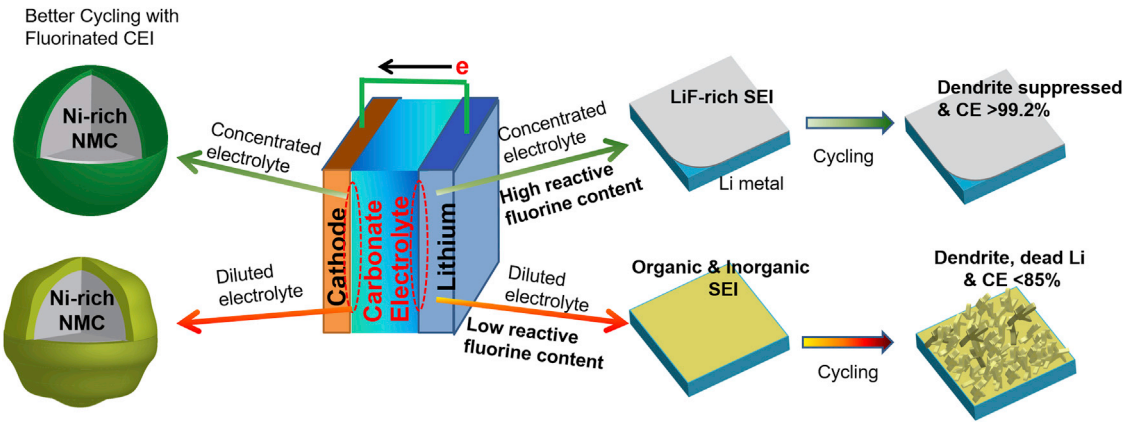

Figure 1. Schematic Illustration of the Effect of the Reactive Fluorine Content in the Concentrated Carbonate Electrolyte on a Li-Metal Anode and Ni-Rich Cathode

than those of carbonate-based electrolytes. Thus, ether-based electrolytes can only be applied in low-voltage systems such as Li-S, Li-O_2, and Li-$LiFePO_4$.[18,22,32,34] For high energy density LMBs that require Li metal to be paired with a high-voltage, high-capacity cathode such as Ni-rich cathodes, a non-ether electrolyte that can simultaneously stabilize both Li-metal and cathode surfaces must be developed.

Organic carbonates are exclusively used as electrolyte solvents in almost all commercial LIBs today thanks to their intrinsically high oxidation stability (>4.3 V) and their unique capabilities of forming protective interphases on graphite anodes. However, these electrolytes cannot accommodate the much more stringent requirements presented when graphite and mild transition metal oxides (such as $LiCoO_2$) are replaced by the more aggressive Li-metal and Ni-rich NMC (nickel-manganese-cobalt) materials.[2,10,12,24] Here, we report that by simply increasing the Li bis(fluorosulfonyl)imide (LiFSI) concentration in carbonate electrolytes (propylene carbonate [PC], dimethyl carbonate [DMC], ethylene carbonate [EC]/DMC), a significantly high CE of ~99.3% can be achieved with an extremely high cycling stability. The LiF-rich solid-electrolyte interphase (SEI) layer, which is formed mainly from the LiFSI salt reduction, effectively prevents dendrite growth and minimizes the sustained electrolyte decomposition. These highly concentrated electrolytes also stabilize the high-capacity Ni-rich NMC cathode at higher voltage (Figure 1). The simultaneous stabilization of both anode and cathode surfaces in these electrolytes leads to a high energy density NMC||Li cell, which steadily delivers high energy density at a high cutoff voltage (4.6 V) for extended cycles.

RESULTS AND DISCUSSION

CE truthfully monitors utilization and dendrite formation of metallic Li. A low CE indicates significant consumption of Li^+ and electrolyte, which will irreversibly result in poor cycling stability and the end of cell life. Li plating/stripping CE, defined as the ratio between the amounts of Li stripped and the amount plated on the Cu substrate, was examined in different electrolytes in 2,032 coin cells. Figures 2A–2D show the voltage profiles of the Cu||Li cells at a current density of 0.2 mA/cm^{-2} in LiFSI-DMC electrolytes at varying salt concentrations. The charge-discharge voltage hysteresis and ionic conductivity of different electrolytes are summarized in Figure 2E, and the Li plating/stripping CEs in different electrolytes are compared in Figure 2F. Here, M stands for molar concentration, i.e., mole of salt dissolved in a liter of solvent. In diluted electrolyte (2 M LiFSI-DMC), the CE is only about 20%, indicating

[1]Department of Chemical and Biomolecular Engineering, University of Maryland, College Park, MD 20740, USA

[2]School of Optical and Electronic Information, Huazhong University of Science and Technology, Wuhan, Hubei 430074, China

[3]Electrochemistry Branch, Power and Energy Division Sensor and Electron Devices Directorate, US Army Research Laboratory, Adelphi, MD 20783, USA

[4]Lead Contact

*Correspondence: cswang@umd.edu

https://doi.org/10.1016/j.chempr.2017.10.017

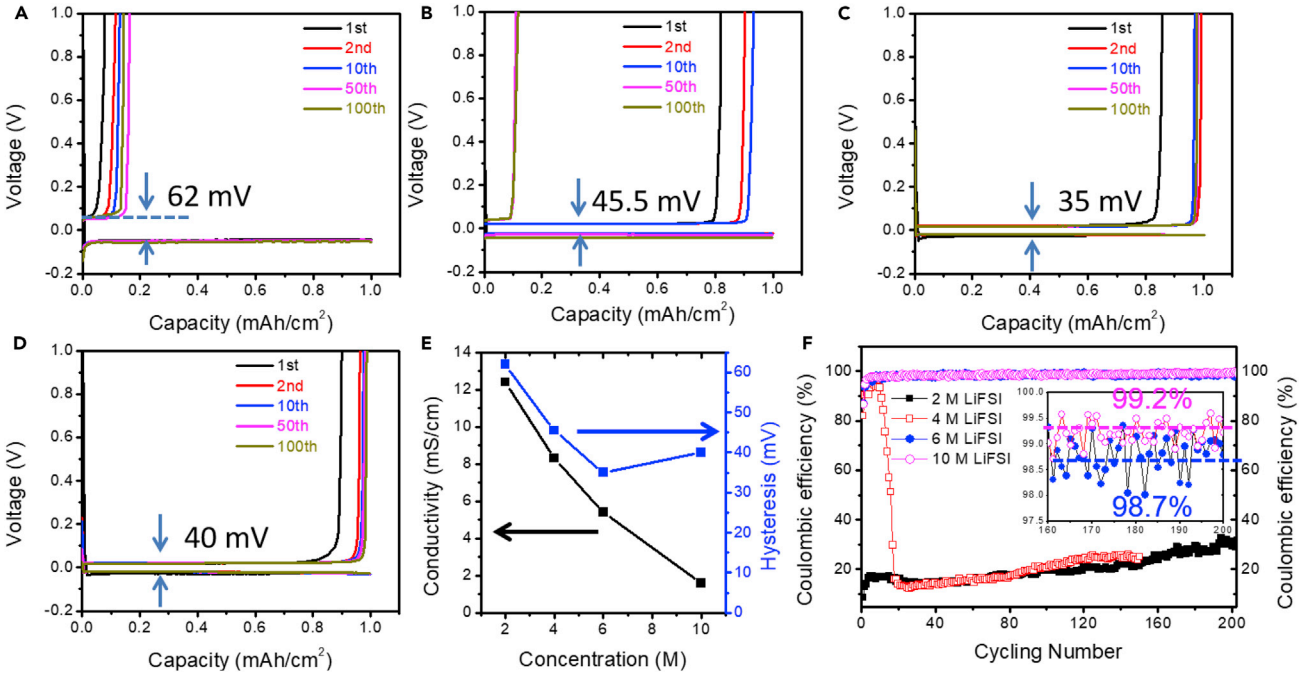

Figure 2. Electrochemical Performance of Li-Metal Plating/Stripping on a Cu Working Electrode in LiFSI-DMC Electrolytes with Different Salt Concentrations

(A–D) Voltage profiles for the cell cycled in 2 M LiFSI-DMC (A), 4 M LiFSI-DMC (B), 6 M LiFSI-DMC (C), and 10 M LiFSI-DMC (D).

(E) Conductivity for the different concentrated LiFSI-DMC electrolytes and hysteresis of Li plating/stripping on a Cu working electrode in different concentrations of electrolytes.

(F) Coulombic efficiency of Li plating/stripping in LiFSI-DMC electrolyte with different concentrations. The plating/stripping current density is 0.2 mA/cm^2.

significant irreversible consumption of both Li^+ and electrolyte solvent as a result of the poor protection provided by the interphase, as revealed in the previous studies.[10] As the LiFSI concentration increases from 2 to 6 M, the CE quickly increased from 20% to 98.7%, eventually reaching 99.2% at 10 M, which is the highest CE ever reported for Li-metal anodes. Equally important is the overpotential between the plating and stripping processes, which becomes much lower in the concentrated carbonate electrolytes, despite their lower bulk ion conductivity than that of diluted electrolytes (Figure 2E), revealing that the interfacial resistances are dramatically reduced as a result of the high salt concentration. As a result of the improved CE and reduced interfacial resistances, the cycling stability of the Li anode in concentrated electrolytes improves dramatically. Although the CE in diluted electrolyte (2 M) never reached >40%, a relatively high CE of about 96% could by obtained in 4 M LiFSI-DMC electrolyte during the initial cycles. However, this CE lasted for only about ten cycles and then dropped to about 20%, which is similar to the diluted electrolyte (Figures 2B and 2F). In sharp comparison, 6 M and 10 M LiFSI-DMC electrolytes enabled up to 200 cycles without any deterioration detected. The Li plating/stripping behavior in Li/Li symmetrical cells was also evaluated in 6 M and 10 M LiFSI-DMC electrolytes (Figure S1). Both electrolytes showed good cycling stability. However, the overpotential in 6 M electrolyte increased at a faster pace than that in 10 M electrolyte. After 250 cycles, the overpotential in 6 M electrolyte was higher.

The highly reversible nature of Li plating/stripping in concentrated electrolytes is still preserved after DMC is replaced with other carbonate solvents, as shown in Figure 3

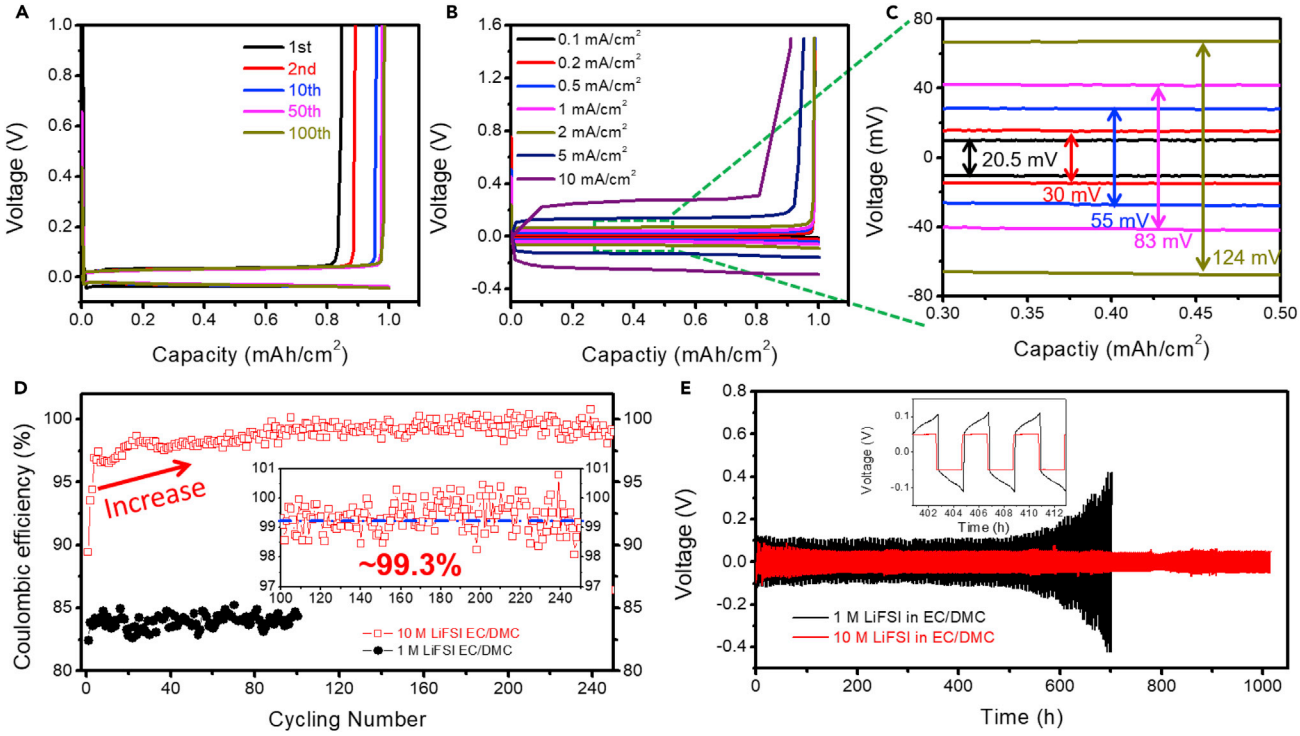

Figure 3. Electrochemical Performance of Li-Metal Plating/Stripping in 10 M LiFSI-EC/DMC (EC:DMC = 1:1 by Volume) Electrolyte

(A) Voltage profiles for the cell cycled at a current of 0.5 mA/cm^2.

(B) Polarization of the plating/stripping for 10 M LiFSI-EC/DMC electrolyte with different current densities.

(C) Enlargement of (B) in the capacity of 0.30–0.50 mAh/cm^2.

(D) CE of Li deposition/stripping in 1 M LiFSI-EC/DMC and 10 M LiFSI-EC/DMC at a current of 0.2 mA/cm^2.

(E) Li-metal plating/stripping from a Li||Li cell cycled at 1 mA/cm^2.

(LiFSI-EC/DMC system) and Figure S2 (LiFSI PC system). At 0.2 mA/cm^{-2}, an overpotential of about 10.2 mV (hysteresis, ~20.5 mV) was observed for LiFSI-EC/DMC (Figures 3B and 3C), which increased to ~62 mV and 100 mV at a current density of 2 and 5 mA/cm^{-2}, respectively. These values representing rate capability are comparable with concentrated DME ether electrolyte.[4] The Li plating/stripping CEs in the 1 M EC/DMC and the 10 M EC/DMC are compared in Figure 3D. A significantly higher CE of 97.5% is achieved in the initial cycles in the 10 M LiFSI-EC/DMC, which gradually ramps up to ~99.3% after about 80 cycles. Again, this value remains the highest among all the reported Li-metal anode materials. In sharp contrast, the diluted electrolyte shows only a reversible CE of ~84% for EC/DMC and ~78% for PC (Figure S2).

We also assembled symmetric Li||Li cells to further confirm the cycling stability of Li-metal anode in an EC/DMC system. The long-term cycling stabilities of coin-type Li||Li cells in 10 M and 1 M LiFSI-EC/DMC electrolytes are compared in Figure 3E. The interfacial resistance of the Li||Li cell in concentrated electrolyte decreased in the first 60 hr, and then remained constant without any overpotential increase in the following 1,000 hr. However, the identical Li||Li cells in the diluted electrolyte cycled at the same current density demonstrated a significant impedance increase after only about 500 hr. After 700 hr, the overpotential of the cell was almost ten times higher than that using the concentrated electrolyte. The stripping/plating capacities (2 mAh/cm^2) in the Li||Li cell generally meet the requirements of commercial Li batteries imposed on the anodes in terms of areal capacity,

current density, and cycle life.[37] These results further suggest that the better cyclability of Li-metal anodes in concentrated electrolytes could come from a more robust interphase that inhibits Li-metal dendrite growth and minimizes consumption of the electrolytes.

Spectroscopic studies were conducted to understand the mechanism of high CE brought about by concentrated electrolytes. Raman spectra in Figures S3–S7 revealed that as the LiFSI salt concentration increases, the free carbonate molecules and free FSI^- are dramatically decreased. To establish whether a relationship exists between the coordinated carbonate solvent with CE, 8.5 M LiTFSI-DMC, in which almost all DMC molecules were coordinated with Li^+ (Figure S8), was also studied as a comparison. Expectedly, the DMC structure in this electrolyte is quite similar to that in 10 M LiFSI concentrated electrolyte. However, a significantly lower Li plating/stripping CE arose from the LiTFSI concentrated electrolyte (~30%; Figure S9). Therefore, the different Li plating/stripping behaviors between 10 M LiFSI and 8.5 M LiTFSI electrolytes must come from the different interphase chemistry originating from the salt anion. We also evaluated the CE of Li plating and stripping in a saturated $LiPF_6$ EC/DMC electrolyte (<5 M) and highly concentrated LiFTFSI ($Li[(FSO_2)N(SO_2CF_3)]$) EC/DMC electrolyte (8 M). Both electrolytes showed an improved CE for Li plating and stripping. However, because of the lower solubility of $LiPF_6$ in EC/DMC (Figure S10), the CE for Li plating and striping increased from 82% for 1 M $LiPF_6$ electrolyte to only ~91% at the saturation of $LiPF_6$ (Figure S11), whereas the CE can reach >98.5% for 8 M LiFTFSI EC/DMC electrolyte (Figure S12), which is significantly higher than the Li plating/stripping CE (30%) in 8.5 M LiTFSI electrolytes. This difference arises from the much higher reactivity of LiFSI and LiFTFSI than LiTFSI, which accordingly results in much higher F content in the SEI on the Li-metal surface.[31]

LiFSI concentrations significantly affected the morphology of the cycled Li metals. Scanning electron microscopy (SEM) images in Figures 4A–4D compare the Li-metal surfaces after being cycled at a current density of 0.5 mA/cm^2 and areal capacity of 1 mAh/cm^2 for 100 cycles in different electrolytes (1 M LiFSI and 10 M LiFSI-EC/DMC). Significant amount of Li dendrites as well as dead Li formed on the surface of the Li-metal anode during cycling in the diluted electrolyte, which is similar to the morphology of Li metal cycled in the other carbonate electrolytes.[26,29] The formation of needle-like dendrites with diameter of 200–400 nm and length of several micrometers leads to an explosive increase in the specific surface area of the Li-metal anode, which accelerates the parasitic reactions with electrolyte and exhausts the Li sources, resulting in not only poor efficiencies of LMBs and extremely low volume-specific capacities of the Li-metal anodes[38] but also severe safety hazards. The Li foil (Figure 4A, inset) and the Cu electrode (Figure S13) after being cycled in 1 M LiFSI-EC/DMC electrolyte were found to be covered by a polymer-like brown film, indicating that the interphase formed in dilute carbonate electrolyte might mainly be contributed by the massive reduction of solvents.[37] This observation suggests that the poor protection by the interphase likely originates from its organic nature, which is ineffective in shielding bulk Li metal against sustained electron tunneling at certain "hot-spots," leading to sustained electrolyte reduction and preferential Li growth, as demonstrated by a CE of <85% (Figure 3D). In contrast, the surfaces of the Li-metal and Cu electrode turn black after cycling in concentrated carbonate electrolyte, indicating that the composition and the morphology of the SEI layer in concentrated carbonate electrolyte differs from the SEI formed in diluted electrolyte.[4] The Li surface cycled in the concentrated carbonate electrolyte displays a round-shaped morphology with a dense and uniform structure

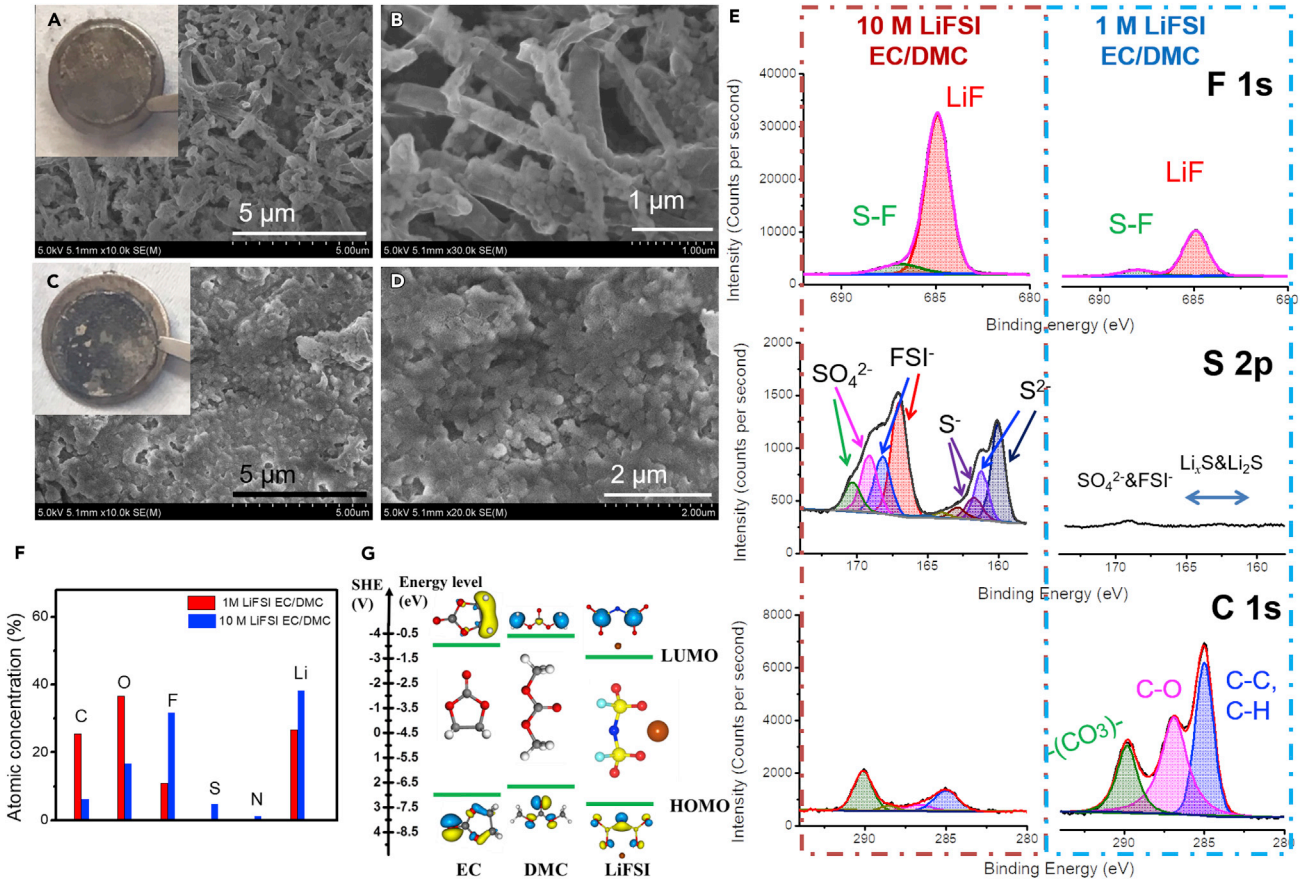

Figure 4. Morphology of Cycled Li and the SEI Analysis

(A–D) SEM images of cycled Li-metal anodes obtained from 1 M LiFSI EC/DMC (EC:DMC = 1:1) (A and B) and from 10 M LiFSI EC/DMC (C and D). Insets in (A) and (C) show the optical images of cycled Li foils on the spacers.

(E) XPS analysis of the SEI layers for the Li-metal anode cycled in concentrated EC/DMC and diluted EC/DMC electrolyte. F1s, S2p, and C1s spectra are presented, including peak deconvolution and assignments.

(F) The elemental concentration of the SEI layer obtained in the XPS analysis for the two Li-metal anodes.

(G) The LUMO and HOMO energy values of the solvents and the salt obtained by DFT simulations.

(Figures 4C and 4D). Such morphology of Li deposition enabled by concentrated electrolytes should render three notable advantages to the LMBs: (1) The severe safety concern induced by dendritic and dead Li can be significantly relieved. Differing from the needle-like dendrites deposited in diluted electrolyte, which are a few hundred nanometers long and could easily penetrate the separators, the round-shaped structures reduce the possibility of penetration of the porous separators. (2) The surface area of the Li deposited in concentrated electrolyte is much smaller, hence minimized side reactions between the deposited Li and the electrolyte lead to a much higher Li deposition/stripping CE (as shown in Figures 2 and 3). (3) A much higher volumetric capacity would be available from the dense packing of Li metal upon its deposition from the concentrated carbonate electrolyte.

X-ray photoelectron spectroscopy (XPS) analysis revealed the chemical compositions of the interphase formed on the Li-metal surface in different electrolytes (Figures 4E and S14). The differences in the F1s, S2p, C1s, and O1s spectra between the two Li-metal anodes that were cycled in diluted and concentrated electrolytes are pronounced. One major difference lies in the significant variations in the elemental

compositions in these two interphases. The one formed in the concentrated electrolyte is characterized by much higher F and S content but lower C and O content than those of the one formed in dilute electrolytes. The atomic ratio of F:C in the interphase is dramatically increased by more than ten times, from 0.42 in diluted electrolyte to over 5.05 in the concentrated electrolyte. More specifically, the accumulation of LiF species in the interphase is accompanied by the decline of carbon and oxygen species (C–C, C–H, C–O, C=O, etc.) on the Li-metal surface. Therefore, we can tentatively conclude that, because of the high population of FSI anions and their reactivity against reduction, the interphase formed by concentrated electrolyte tends to contain more LiF, which is contributed by the reduction of FSI rather than by solvent molecules. It is this chemical difference that is responsible for the distinct Li deposition/stripping behavior observed. LiF with high interface energy to Li can effectively prevent Li dendrite growth.[3]

Molecular orbital energies of EC, DMC, and LiFSI were calculated by density functional theory (DFT) with the purpose of further understanding their respective reaction pathways. Figure 4G shows the energy values of the lowest unoccupied molecular orbital (LUMO) and the highest occupied molecular orbital (HOMO) for those species. LiFSI has a lower LUMO energy (−1.70 eV) than those of EC (−0.92 eV) and DMC (−0.54 eV), indicating its higher tendency to react with Li metal than that of the solvent molecules under standard conditions. The preferential reduction of FSI^- by Li metal is dramatically enhanced as the molar ratio between solvent and salt decreases from 9.5 in diluted electrolyte to 0.95 in concentrated electrolyte. In addition to thermodynamic considerations, the $–SO_2F$ group in FSI^- is also kinetically more reactive than the carbonate solvents toward the Li-metal anode.[39] Splitting F^- by cleavage of S–F bond leads to a thermodynamically stable LiF first, which precipitates on the Li-metal surface, followed by cleavage of the S–N bond. The broken fragment of $F(SO_2)_2N$ under the strong attraction of oxygen atoms to the Li surface leads to the formation of SO_2, which promptly leaves the surface as a result of blocking by the LiF dominating layer formed earlier. This could be the main reason for the scarcity of sulfur-containing species in comparison with LiF (Figure 4F). Consequently, a LiF-rich interphase is formed in the highly concentrated LiFSI carbonate electrolyte, as demonstrated by the XPS results (Figures 4E and 4F). LiF plays two critical roles in increasing the CE: (1) LiF itself is a good electric insulator and effectively blocks electron leakage through the interphase,[40] which was believed to be detrimental and one of the critical reasons causing sustained electrolyte decomposition and dendrite formation.[41,42] (2) LiF exhibits much higher interfacial energy to Li metal and meanwhile produces a reduction of as much as 0.13 eV in the activation energy barrier for Li diffusion at the electrolyte/Li-metal electrode interface.[43] Thus, the surface diffusivity should be increased by more than two orders of magnitude, which facilitates Li transport along the interface and promotes the formation of a uniform morphology of the deposited Li metal. This is consistent with the recent reports[44–47] that LiF can effectively suppress Li dendrite formation.

An ideal electrolyte for LMBs should not only provide a high Li plating/stripping CE but also be stable against oxidation on high-voltage cathode surfaces. Figure 5A demonstrates the anodic linear sweep of three different electrolytes (1 M LiFSI in EC/DMC, 10 M LiFSI in EC/DMC, and 4 M LiFSI-DME) from 3.0 V to 6.5 V at a scanning rate of 10 mV/s. At a high potential of 5.0 V, the anodic current density in 10 M LiFSI-EC/DMC electrolyte is only 1/100 that of 4 M LiFSI-DME or 1/7 that of 1 M LiFSI-EC/DMC electrolyte. As indicated by Dahn et al.,[48] the oxidation of carbonate solvents (especially EC) at a high voltage is usually responsible for impedance

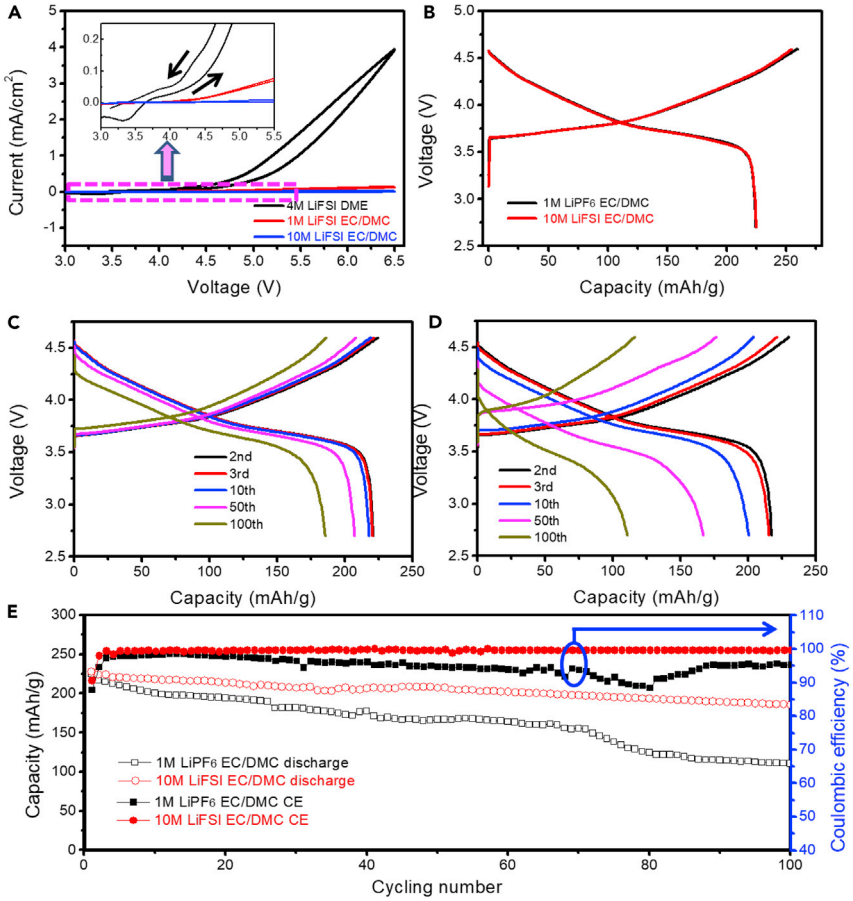

Figure 5. Electrochemical Performance of NMC622||Li LMBs in 10 M LiFSI EC/DMC and 1 M $LiPF_6$ EC/DMC Electrolytes

(A) Oxidation stabilities for different electrolytes. The scanning rate is 10 mV/s.

(B) The first charge-discharge profiles of NMC622||Li batteries in the two electrolytes.

(C) Charge-discharge profiles of NMC622||Li batteries in 10 M LiFSI EC/DMC electrolyte.

(D) Charge-discharge profiles of NMC622||Li batteries in 1 M $LiPF_6$ EC/DMC electrolyte.

(E) Cycling performance of NMC622||Li batteries in these two electrolytes with 2.7–4.6 V cutoff voltage.

growth and cell failure. The excellent oxidation stability of concentrated LiFSI-EC/DMC electrolyte can be ascribed to the following two reasons: (1) the less stable organic component in possible cathode interphase is largely reduced because of the much lower presence of solvent in the concentrated electrolytes (Figure S15); and (2) a fluorine-rich interphase, which is mainly from anion oxidation, passivates the cathode surface and stabilizes the electrolyte solvents (Figure S16). According to XPS, the ratio of F:C (4.1) on such a stabilized cathode surface is significantly higher than the cathode surface cycled in 1 M $LiPF_6$ EC/DMC electrolyte (0.65). These F-containing species, including LiF, CF_x, and S–F, form a dense cathode interphase, suppressing the parasitic reactions between the cathode and the electrolyte.

The charge-discharge and cycling behaviors of NMC622||Li cells using different electrolytes were investigated (Figures 5B–5E and S17–S21). To utilize the high capacity of NMC, we adopted a much harsher charge-discharge protocol with a cut-off voltage of 4.6 V, which is much higher than most common charging protocols

with a low cutoff voltage of 4.2 or 4.3 V using conventional electrolytes. Such a high cutoff voltage presents a rather rigorous test on the anodic stability of the electrolytes because it applies very severe electrochemical stress to induce side reactions. NMC622||Li cells in 4 M LiFSI-DME cannot be charged to >4.2 V because of the poor anodic stability of ether solvents (Figure S17) although they possess a high Li-metal plating/stripping CE of ~99% (Figure S18). In the diluted 1 M LiFSI-EC/DMC electrolyte, serious corrosion of the Al current collector by LiFSI (Figure S19) also make the first charge of NMC622 impossible (Figure S20). Because the charging of NMC622||Li cells in 1 M LiFSI-EC/DMC and 4 M LiFSI-DME failed between 2.7 and 4.6 V, the cycling behavior of NMC622||Li cells in highly concentrated 10 M LiFSI-EC/DMC electrolyte was compared with that of 1 M LiPF6 EC/DMC electrolyte (Figures 5B–5E).

Almost identical electrochemical performances can be obtained from the first cycle of NMC622||Li cells in both diluted $LiPF_6$ electrolyte and the high concentration LiFSI carbonate electrolytes (Figure 5B). The slightly lower initial CE in 1 M $LiPF_6$ EC/DMC might be because of the oxidation of the carbonate solvents at the high voltage. Figures 5C and 5D show the charge-discharge voltage profiles at different cycles. Much higher voltage polarization with significant capacity decay was observed for the cell using 1 M $LiPF_6$ EC/DMC, suggesting that higher resistance was generated at the electrode interfaces as a result of the decomposition of the electrolyte solvent. Cycling performance and the corresponding CE of NMC622||Li cells using these two different electrolytes are shown for the first 100 cycles (Figure 5E). The cell in 1 M $LiPF_6$ EC/DMC exhibited a CE of about 99% in the first 20 cycles. However, starting from the 20th cycle, this CE sharply dropped to only about 95%, accompanied by a faster capacity decay rate. After 100 cycles, the cell in 1 M $LiPF_6$ EC/DMC retained only ~52% of its original capacity. In contrast, the concentrated EC/DMC electrolyte enabled a high-energy-density NMC622||Li cell with high and stable CE of >99.6% along with a capacity retention of ~86% after 100 cycles, which represents a significant improvement for the aggressive chemistry of both Li-metal and NMC622 over traditional carbonate electrolytes, even with such a limited number of cycles. The enhancement in the electrochemical performance of NMC622||Li cells in concentrated carbonate electrolytes is universal. Similar improvements in cycling performance were achieved for concentrated DMC electrolyte (Figure S21). After 150 cycles, the cell in concentrated DMC electrolyte retained a capacity of ~80%. Yet, the cell in the dilute 1 M $LiPF_6$ DMC electrolyte dramatically dropped to 19% of the initial capacity.

EXPERIMENTAL PROCEDURES

Materials

Cathode NMC622 ($LiNi_{0.6}Mn_{0.2}Co_{0.2}O_2$) electrode laminates (~13 mg active material cm^{-2}) were supplied by SAFT America. The electrode laminates were punched into discs and further dried at 80°C under a vacuum overnight. All the solvents were purchased from Sigma-Aldrich, including EC, DMC, and PC. All the solvents were dried by molecular sieve (4 Å, Sigma-Aldrich) to make sure the water content was lower than 2 ppm, which was tested by a Karl-Fisher titrator (Metrohm 899 Coulometer). Lithium bis(fluorosulfonyl)imide (LiFSI, 99.9%) was purchased from American Elements. $LiPF_6$ (>99.99%) was purchased from Sigma-Aldrich.

Material Characterization

The morphology and microstructure of the samples were investigated by SEM (Hitachi SU-70). XPS was conducted on a high-sensitivity Kratos AXIS 165 X-ray photoelectron spectrometer with Mg Kα radiation. All binding energy values were

referenced to the C 1s peak of carbon at 284.6 eV. Before XPS characterization, the cycled electrodes were washed with the corresponding solvents several times to remove residual salts.

Electrochemical Measurements

Electrolytes are prepared by adding LiFSI or $LiPF_6$ into various anhydrous solvents (DMC, PC, EC/DMC). The charge-discharge performances of the LMBs were examined by 2,032 coin-type cells. The same coin-type cells were used to investigate the cycling stability of Li plating/stripping in different electrolytes. The CE of Li plating and stripping was calculated from the ratio of the Li removed from the Cu substrate to that deposited in the same cycle. A three-electrode "T cell" was utilized to test the stability window of the different electrolytes with polished stainless steel as the working electrode and Li foils as the reference and counter electrodes with a Gamry 1000E electrochemical workstation (Gamry Instruments, USA). All cells were assembled in a glove box with water and oxygen content lower than 2 ppm and were tested at room temperature. The galvanostatic charge-discharge test was conducted on an Arbin battery test station (BT2000, Arbin Instruments, USA).

DFT Calculations

The Vienna ab initio Simulation Package (VASP) was used to perform DFT calculations,[49,50] and Perdew-Bruke-Ernzerhof (PBE) functional of the generalized-gradient approximation (GGA) was used for electron exchange and correlation.[51] Previous works have shown that GGA-PBE yields qualitatively the same trend for the ground state of higher acenes as the B3LYP function and a high-level wave function method.[52] The projector augmented wave method with an energy cutoff of 580 eV was used to describe the ion-electron interaction on a single *k* point.[53] The convergence condition for the energy was 10^{-5} eV, and the structures were relaxed until the force on each atom was less than 0.001 eV/Å. For all solvents and the salt, a vacuum larger than 15 Å was used to simulate the molecules. Visualization of the LUMO and HOMO was done with Molekel software.[54]

SUPPLEMENTAL INFORMATION

Supplemental Information includes 21 figures and can be found with this article online at https://doi.org/10.1016/j.chempr.2017.10.017.

AUTHOR CONTRIBUTIONS

Conceptualization, X.F. and C.W.; Methodology, X.F., L.C., X.J., and K.X.; Investigation, X.F., L.C., T.D., S.H., J.C., J.Z., and F.W.; Software, X.J. and J.J.; Writing – Original Draft, X.F.; Writing – Review & Editing, K.X. and C.W.; Funding Acquisition, C.W.; Supervision, C.W.

ACKNOWLEDGMENTS

This work was supported as part of the Nanostructures for Electrical Energy Storage, an Energy Frontier Research Center funded by the Basic Energy Sciences program of the US Department of Energy Office of Science under award number DESC0001160. We acknowledge the support of the Maryland NanoCenter and its AIM Lab.

Received: August 29, 2017
Revised: October 15, 2017
Accepted: October 27, 2017
Published: December 14, 2017

REFERENCES AND NOTES

1. Armand, M., and Tarascon, J.M. (2008). Building better batteries. Nature *451*, 652–657.
2. Lin, D., Liu, Y., and Cui, Y. (2017). Reviving the lithium metal anode for high-energy batteries. Nat. Nanotechnol. *12*, 194–206.
3. Lu, Y., Tu, Z., and Archer, L.A. (2014). Stable lithium electrodeposition in liquid and nanoporous solid electrolytes. Nat. Mater. *13*, 961–969.
4. Qian, J., Henderson, W.A., Xu, W., Bhattacharya, P., Engelhard, M., Borodin, O., and Zhang, J.-G. (2015). High rate and stable cycling of lithium metal anode. Nat. Commun. *6*, 6362.
5. Wood, K.N., Noked, M., and Dasgupta, N.P. (2017). Lithium metal anodes: toward an improved understanding of coupled morphological, electrochemical, and mechanical behavior. ACS Energy Lett. *2*, 664–672.
6. Cheng, X.-B., Zhang, R., Zhao, C.-Z., Wei, F., Zhang, J.-G., and Zhang, Q. (2016). A review of solid electrolyte interphases on lithium metal anode. Adv. Sci. *3*, 1500213.
7. Cheng, X.-B., Zhang, R., Zhao, C.-Z., and Zhang, Q. (2017). Toward safe lithium metal anode in rechargeable batteries: a review. Chem. Rev. *117*, 10403–10473.
8. Choudhury, S., Mangal, R., Agrawal, A., and Archer, L.A. (2015). A highly reversible room-temperature lithium metal battery based on crosslinked hairy nanoparticles. Nat. Commun. *6*, 10101.
9. Aurbach, D., Zinigrad, E., Cohen, Y., and Teller, H. (2002). A short review of failure mechanisms of lithium metal and lithiated graphite anodes in liquid electrolyte solutions. Solid State Ionics *148*, 405–416.
10. Ding, F., Xu, W., Chen, X., Zhang, J., Engelhard, M.H., Zhang, Y., Johnson, B.R., Crum, J.V., Blake, T.A., Liu, X., and Zhang, J.-G. (2013). Effects of carbonate solvents and lithium salts on morphology and coulombic efficiency of lithium electrode. J. Electrochem. Soc. *160*, A1894–A1901.
11. Jeong, S.-K., Seo, H.-Y., Kim, D.-H., Han, H.-K., Kim, J.-G., Lee, Y.B., Iriyama, Y., Abe, T., and Ogumi, Z. (2008). Suppression of dendritic lithium formation by using concentrated electrolyte solutions. Electrochem. Commun. *10*, 635–638.
12. Xu, W., Wang, J., Ding, F., Chen, X., Nasybulin, E., Zhang, Y., and Zhang, J.-G. (2014). Lithium metal anodes for rechargeable batteries. Energy Environ. Sci. *7*, 513–537.
13. Xu, K. (2004). Nonaqueous liquid electrolytes for lithium-based rechargeable batteries. Chem. Rev. *104*, 4303–4418.
14. Li, W., Yao, H., Yan, K., Zheng, G., Liang, Z., Chiang, Y.-M., and Cui, Y. (2015). The synergetic effect of lithium polysulfide and lithium nitrate to prevent lithium dendrite growth. Nat. Commun. *6*, 7436.
15. Li, N.-W., Yin, Y.-X., Yang, C.-P., and Guo, Y.-G. (2016). An artificial solid electrolyte interphase layer for stable lithium metal anodes. Adv. Mater. *28*, 1853–1858.
16. Kazyak, E., Wood, K.N., and Dasgupta, N.P. (2015). Improved cycle life and stability of lithium metal anodes through ultrathin atomic layer deposition surface treatments. Chem. Mater. *27*, 6457–6462.
17. Cheng, X.-B., Hou, T.-Z., Zhang, R., Peng, H.-J., Zhao, C.-Z., Huang, J.-Q., and Zhang, Q. (2016). Dendrite-free lithium deposition induced by uniformly distributed lithium ions for efficient lithium metal batteries. Adv. Mater. *28*, 2888–2895.
18. Liu, K., Pei, A., Lee, H.R., Kong, B., Liu, N., Lin, D., Liu, Y., Liu, C., Hsu, P.-c., Bao, Z., and Cui, Y. (2017). Lithium metal anodes with an adaptive "solid-liquid" interfacial protective layer. J. Am. Chem. Soc. *139*, 4815–4820.
19. Lin, D., Liu, Y., Liang, Z., Lee, H.-W., Sun, J., Wang, H., Yan, K., Xie, J., and Cui, Y. (2016). Layered reduced graphene oxide with nanoscale interlayer gaps as a stable host for lithium metal anodes. Nat. Nano *11*, 626–632.
20. Zheng, G., Lee, S.W., Liang, Z., Lee, H.-W., Yan, K., Yao, H., Wang, H., Li, W., Chu, S., and Cui, Y. (2014). Interconnected hollow carbon nanospheres for stable lithium metal anodes. Nat. Nano *9*, 618–623.
21. Yang, C.-P., Yin, Y.-X., Zhang, S.-F., Li, N.-W., and Guo, Y.-G. (2015). Accommodating lithium into 3D current collectors with a submicron skeleton towards long-life lithium metal anodes. Nat. Commun. *6*, 8058.
22. Yun, Q., He, Y.-B., Lv, W., Zhao, Y., Li, B., Kang, F., and Yang, Q.-H. (2016). Chemical dealloying derived 3D porous current collector for Li metal anodes. Adv. Mater. *28*, 6932–6939.
23. Kim, J.-S., Kim, D.W., Jung, H.T., and Choi, J.W. (2015). Controlled lithium dendrite growth by a synergistic effect of multilayered graphene coating and an electrolyte additive. Chem. Mater. *27*, 2780–2787.
24. Ding, F., Xu, W., Graff, G.L., Zhang, J., Sushko, M.L., Chen, X., Shao, Y., Engelhard, M.H., Nie, Z., Xiao, J., et al. (2013). Dendrite-free lithium deposition via self-healing electrostatic shield mechanism. J. Am. Chem. Soc. *135*, 4450–4456.
25. Zhang, S.S. (2006). A review on electrolyte additives for lithium-ion batteries. J. Power Sources *162*, 1379–1394.
26. Qian, J., Xu, W., Bhattacharya, P., Engelhard, M., Henderson, W.A., Zhang, Y., and Zhang, J.-G. (2015). Dendrite-free Li deposition using trace-amounts of water as an electrolyte additive. Nano Energy *15*, 135–144.
27. Zhang, X.-Q., Cheng, X.-B., Chen, X., Yan, C., and Zhang, Q. (2017). Fluoroethylene carbonate additives to render uniform Li deposits in lithium metal batteries. Adv. Funct. Mater. *27*, 1605989.
28. Zhou, D., Liu, R., He, Y.-B., Li, F., Liu, M., Li, B., Yang, Q.-H., Cai, Q., and Kang, F. (2016). SiO_2 hollow nanosphere-based composite solid electrolyte for lithium metal batteries to suppress lithium dendrite growth and enhance cycle life. Adv. Energy Mater. *6*, 1502214.
29. Yu, H., Zhao, J., Ben, L., Zhan, Y., Wu, Y., and Huang, X. (2017). Dendrite-free lithium deposition with self-aligned columnar structure in a carbonate–ether mixed electrolyte. ACS Energy Lett. *2*, 1296–1302.
30. Qian, J., Adams, B.D., Zheng, J., Xu, W., Henderson, W.A., Wang, J., Bowden, M.E., Xu, S., Hu, J., and Zhang, J.-G. (2016). Anode-free rechargeable lithium metal batteries. Adv. Funct. Mater. *26*, 7094–7102.
31. Miao, R., Yang, J., Feng, X., Jia, H., Wang, J., and Nuli, Y. (2014). Novel dual-salts electrolyte solution for dendrite-free lithium-metal based rechargeable batteries with high cycle reversibility. J. Power Sources *271*, 291–297.
32. Miao, R., Yang, J., Xu, Z., Wang, J., Nuli, Y., and Sun, L. (2016). A new ether-based electrolyte for dendrite-free lithium-metal based rechargeable batteries. Sci. Rep. *6*, 21771.
33. Zhang, R., Chen, X.-R., Chen, X., Cheng, X.-B., Zhang, X.-Q., Yan, C., and Zhang, Q. (2017). Lithiophilic sites in doped graphene guide uniform lithium nucleation for dendrite-free lithium metal anodes. Angew. Chem. Int. Ed. *56*, 7764–7768.
34. Ma, Q., Fang, Z., Liu, P., Ma, J., Qi, X., Feng, W., Nie, J., Hu, Y.-S., Li, H., Huang, X., et al. (2016). Improved cycling stability of lithium-metal anode with concentrated electrolytes based on lithium (fluorosulfonyl) (trifluoromethanesulfonyl) imide. ChemElectroChem *3*, 531–536.
35. Park, M.S., Ma, S.B., Lee, D.J., Im, D., Doo, S.-G., and Yamamoto, O. (2014). A highly reversible lithium metal anode. Sci. Rep. *4*, 3815.
36. Erickson, E.M., Markevich, E., Salitra, G., Sharon, D., Hirshberg, D., de la Llave, E., Shterenberg, I., Rosenman, A., Frimer, A., and Aurbach, D. (2015). Review-development of advanced rechargeable batteries: a continuous challenge in the choice of suitable electrolyte solutions. J. Electrochem. Soc. *162*, A2424–A2438.
37. Markevich, E., Salitra, G., Chesneau, F., Schmidt, M., and Aurbach, D. (2017). Very stable lithium metal stripping-plating at a high rate and high areal capacity in fluoroethylene carbonate-based organic electrolyte solution. ACS Energy Lett. *2*, 1321–1326.
38. Aurbach, D. (2000). Review of selected electrode–solution interactions which determine the performance of Li and Li ion batteries. J. Power Sources *89*, 206–218.
39. Budi, A., Basile, A., Opletal, G., Hollenkamp, A.F., Best, A.S., Rees, R.J., Bhatt, A.I., O'Mullane, A.P., and Russo, S.P. (2012). Study of the initial stage of solid electrolyte interphase formation upon chemical reaction of lithium metal and n-methyl-n-propyl-pyrrolidinium-bis(fluorosulfonyl)imide. J. Phys. Chem. C *116*, 19789–19797.
40. Zhang, Q., Pan, J., Lu, P., Liu, Z., Verbrugge, M.W., Sheldon, B.W., Cheng, Y.-T., Qi, Y., and Xiao, X. (2016). Synergetic effects of inorganic components in solid electrolyte interphase on high cycle efficiency of lithium ion batteries. Nano Lett. *16*, 2011–2016.

41. Leung, K., and Budzien, J.L. (2010). Ab initio molecular dynamics simulations of the initial stages of solid-electrolyte interphase formation on lithium ion battery graphitic anodes. Phys. Chem. Chem. Phys. *12*, 6583–6586.

42. Leung, K. (2013). Electronic structure modeling of electrochemical reactions at electrode/electrolyte interfaces in lithium ion batteries. J. Phys. Chem. C *117*, 1539–1547.

43. Deniz, G., Kendra, L.-W., Ravishankar, S., Kathleen, A.S., and Arias, T.A. (2013). The importance of nonlinear fluid response in joint density-functional theory studies of battery systems. Model. Simulat. Mater. Sci. Eng. *21*, 074005.

44. Choudhury, S., and Archer, L.A. (2016). Lithium fluoride additives for stable cycling of lithium batteries at high current densities. Adv. Electron. Mater. *2*, 1500246.

45. Lin, D., Liu, Y., Chen, W., Zhou, G., Liu, K., Dunn, B., and Cui, Y. (2017). Conformal lithium fluoride protection layer on three-dimensional lithium by nonhazardous gaseous reagent freon. Nano Lett. *17*, 3731–3737.

46. Yoo, E., and Zhou, H. (2017). Enhanced cycle stability of rechargeable Li-O_2 batteries by the synergy effect of a LiF protective layer on the Li and DMTFA additive. ACS Appl. Mater. Interfaces *9*, 21307–21313.

47. Zu, C., Azimi, N., Zhang, Z., and Manthiram, A. (2015). Insight into lithium-metal anodes in lithium-sulfur batteries with a fluorinated ether electrolyte. J. Mater. Chem. A *3*, 14864–14870.

48. Xia, J., Liu, Q., Hebert, A., Hynes, T., Petibon, R., and Dahn, J.R. (2017). Succinic anhydride as an enabler in ethylene carbonate-free linear alkyl carbonate electrolytes for high voltage Li-ion cells. J. Electrochem. Soc. *164*, A1268–A1273.

49. Hohenberg, P., and Kohn, W. (1964). Inhomogeneous electron gas. Phys. Rev. *136*, B864–B871.

50. Kohn, W., and Sham, L.J. (1965). Self-consistent equations including exchange and correlation effects. Phys. Rev. *140*, A1133–A1138.

51. Perdew, J.P., Burke, K., and Ernzerhof, M. (1996). Generalized gradient approximation made simple. Phys. Rev. Lett. *77*, 3865–3868.

52. Jiang, D.-e., and Dai, S. (2008). Circumacenes versus periacenes: HOMO–LUMO gap and transition from nonmagnetic to magnetic ground state with size. Chem. Phys. Lett. *466*, 72–75.

53. Blöchl, P.E. (1994). Projector augmented-wave method. Phys. Rev. B *50*, 17953–17979.

54. Portmann, S., and Lüthi, H.P. (2000). MOLEKEL: an interactive molecular graphics tool. CHIMIA Int. J. Chem. *54*, 766–770.